Applied Physics Letters

RESEARCH ARTICLE | MAY 18 2026

Low-loss material for infrared protection of cryogenic quantum applications

Markus Griedel ; Max Kristen ; Biliana Gasharova ; Yves-Laurent Mathis ; Alexey V. Ustinov ; Hannes Rotzinger

Appl. Phys. Lett. 128, 204003 (2026)
https://doi.org/10.1063/5.0323074

Applied Physics Letters ARTICLE pubs.aip.org/aip/apl

Low-loss material for infrared protection of cryogenic quantum applications

Cite as: Appl. Phys. Lett. **128**, 204003 (2026); doi: 10.1063/5.0323074
Submitted: 15 January 2026 · Accepted: 6 April 2026 ·
Published Online: 18 May 2026

View Online Export Citation CrossMark

Markus Griedel,[1,2] Max Kristen,[1,2] Biliana Gasharova,[3] Yves-Laurent Mathis,[3] Alexey V. Ustinov,[1,2] and Hannes Rotzinger[1,2,a)]

AFFILIATIONS

[1]Physikalisches Institut, Karlsruhe Institute of Technology, 76131 Karlsruhe, Germany
[2]Institute for Quantum Materials and Technologies, Karlsruhe Institute of Technology, 76021 Karlsruhe, Germany
[3]Institute for Beam Physics and Technology, Karlsruhe Institute of Technology, 76021 Karlsruhe, Germany

[a)]Author to whom correspondence should be addressed: rotzinger@kit.edu

ABSTRACT

The fragile quantum states of low-temperature quantum applications require protection from infrared radiation caused by higher-temperature stages or other sources. In particular, signal lines have to be manufactured to prevent infrared photons entering through dielectric openings while maintaining low microwave loss. We propose a material system that can efficiently block radiation up to the optical range while transmitting photons at low gigahertz frequencies. It is based on the effect that incident photons are strongly scattered when their wavelength is comparable to the size of particles embedded in a weakly absorbing medium (Mie scattering). The goal of this work is to tailor the absorption and transmission spectrum of an non-magnetic epoxy resin containing sapphire spheres by simulating its dependence on the size distribution. Additionally, we fabricate several material compositions, characterize them, as well as other materials, at optical, infrared, and gigahertz frequencies. In the infrared region (stop band), the attenuation of the Mie scattering optimized material is high and comparable to that of other commonly used filter materials. At gigahertz frequencies (passband), the prototype filter exhibits a high transmission at millikelvin temperatures, with an insertion loss of less than 0.4 dB below 10 GHz.

The low noise environment at ultra-low temperatures in the millikelvin range is a key requirement for many quantum applications, such as semiconducting or superconducting qubits. In particular, the low dissipation of superconducting devices stems from the superconducting energy gap, which suppresses low energy excitations. However, when incident photons with larger energy are absorbed, Cooper pairs get broken, which introduces losses and, consequently, noise. Depending on the application, the performance of superconducting circuits can degrade severely. For instance, SQUID sensors show lower magnetic flux sensitivity, or qubits reduced coherence and energy relaxation time.[1–9] The spectrum of unwanted radiation ranges from optical to infrared (IR) wavelength stemming from room temperature sources and also from lower temperature stages of the cryostat; see Fig. 1(c) for the Planck spectra of several temperature stages. To prevent excess photons, devices must be carefully shielded and are usually enclosed in metallic light-tight boxes, often with several layers.[3,7]

Electrical leads to the superconducting device require a dielectric insulation from the shield. For operation frequencies up to a few tens of gigahertz, coaxial cables are commonly used, with the inner wire insulated from the outer conductor by a dielectric material such as polytetrafluoroethylene (PTFE) or high density polyethylene (HDPE). A drawback of the insulator is that it creates an opening in the otherwise light-tight shield, allowing IR photons to enter the box. An ideal solution to this problem would be to add a low-pass filter to the coaxial cable that ensures lossless transmission at operating frequencies and efficient blocking of IR photons. However, the large range of unwanted photons, which can span over five orders of magnitude up to the far-infrared (FIR) range, makes this a challenging task. Widely used approaches[10–14] employ light-absorbing materials such as Eccosorb.[15] These materials are optimized for efficient, frequency-independent absorption of radiation. While this solution can be highly effective in the blocking band, it also attenuates the signal in the desired passband.

In this paper, we describe an approach in which the properties of a compound of high-quality dielectric sapphire spheres embedded in a polymer (epoxy resin) matrix are utilized. This solution is tailored

to achieve both goals, a very high absorption of infrared radiation and a very low absorption at gigahertz frequencies. The spheres have varying diameters ranging from hundreds of nanometers to hundreds of micrometers. The key idea is that incident radiation interacts strongly with the spheres when the wavelength is comparable to the sphere's diameter, i.e., employing the phenomenon known as Mie scattering. At long wavelengths (several millimeters to centimeters), the interaction is minimal and the wave can pass through.[16,17] We favor a dielectric material system, that is non-magnetic and does not contain any electrically conductive constituents to keep the overall loss low. In particular, sapphire is known for its low microwave loss.[18,19]

The paper is structured as follows. First, the basic principle is introduced, along with simulations based on the Mie theory for strong light–matter interaction. The second part presents and discusses measurement data on the absorption of IR by sapphire spheres embedded in a dielectric matrix. These data are then compared with those of other commonly used materials, such as PTFE, HDPE (transparent and black), Eccosorb CR 124, Stycast 2850 FT, UHU plus Endfest 300 (the primarily used epoxy resin), and UHU plus Endfest 300 loaded with stainless steel or copper powder. The supplementary material contain further details. Finally, we focus on GHz frequency transmission at cryogenic temperatures and present the characteristics of our prototype IR filter.

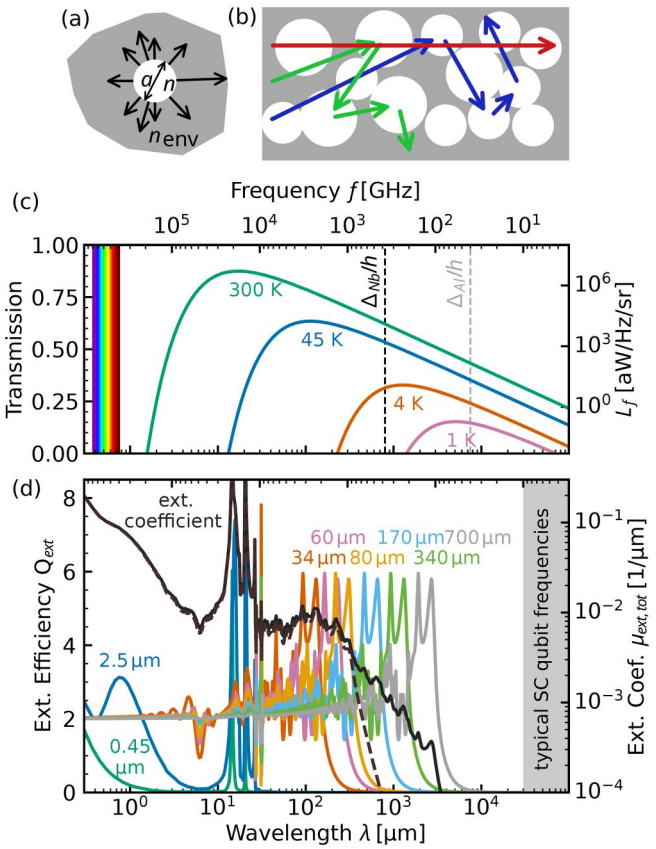

FIG. 1. (a) Scattering at a single sphere ($n = 3.69$; $x = 1.5$) in an epoxy resin matrix ($n_{env} = 1.5$). (b) Spheres of different sizes in an epoxy matrix with scattering path for different wavelengths from short (blue) to long (red) wavelengths. (c) Solid colored lines represent the Planck radiation spectrum of the different cryogenic stages (right axis, L_f); dashed lines indicate the superconducting gap frequencies for niobium (black) and aluminum (gray). The visible light spectrum is indicated on the far left. (d) Calculated Mie scattering for sapphire spheres of varying sizes in an epoxy resin matrix as a function of wavelength (left axis). The black solid (dashed) line is the total extinction efficiency of the composition SP0.45-700 (SP0.45-80) of different sphere sizes (right axis).

The classical Beer–Lambert law[20] $I/I_0 = \exp(-\mu l)$ describes the extinction of radiation with the intensity of outgoing radiation relative to the incoming radiation in media where the interaction is relatively weak and the wavelength of the radiation differs from the internal structure. Here, l is the length of the medium. The extinction coefficient μ can be approximated by $\mu_{abs} + \mu_{sca}$ when considering the absorption and scattering of incident radiation. Due to scattering, the radiation is dispersed in the material (Rayleigh scattering), with a fraction being backscattered. Absorptive losses are converted to heat.

Strong scattering of the incident radiation can be observed when the size parameter $x = \pi a/\lambda$ of the scatterer of diameter a in the medium is on the order of unity. The physics of these processes was worked out by G. Mie and P. Debye and can be found in numerous textbooks (e.g., Refs. 21 and 22).

The total extinction cross section for the particle comprises the energy abstracted from the incident beam by both scattering and absorption $C_{ext} = C_{sca} + C_{abs}$[21] and can be calculated numerically. Our simulation results discussed below are based on the powerful MiePython[23] software package. Figure 1(a) illustrates a calculation of the angle distribution of the scattered radiation. A sapphire sphere ($n = 3.69, a = 50\,\mu$m), embedded in a dielectric matrix (epoxy,[24] $n \approx 1.5$), reacts to incident radiation at $\lambda = 100\ \mu$m by scattering photons almost isotropically. Figure 1(d) shows the extinction efficiency, $Q_{ext} = C_{ext}/\pi(a/2)^2$, for several sphere diameters ranging from 0.45 to 700 μm (individual colors), as a function of the incident wavelength. Except for very small spheres, the general behavior is similar. At wavelengths below 10 μm, Q_{ext} is approximately independent of wavelength. The vibrational mode of sapphire at 10–20 μm is common to all sphere diameters,[25] whereas the position of the resonance at longer wavelengths depends on the individual a and thus on x. Please note the steep decay[22] of the Q_{ext} curves at $x \ll 1$, which drops of as λ^4 (Rayleigh limit).

TABLE I. Parameters for sapphire spheres that are investigated. The wavelength $\lambda_{x'}$ and refractive index components $n(\lambda_{x'})$ and $\kappa(\lambda_{x'})$ are given for $x = 1$. γ is specific for the SP0.45-700 mixture.

A (µm)	$\lambda_{x'}$ (µm)	$n(\lambda_{x'})$	$\kappa(\lambda_{x'})$	γ
0.45	1.41	1.73	1.80×10^{-2}	9.9×10^{-1}
2.5	7.85	1.36	3.43×10^{-2}	5.8×10^{-3}
34	106.8	3.69	3.00×10^{-2}	2.3×10^{-6}
60	188.5	3.69	3.00×10^{-2}	4.2×10^{-7}
80	251.3	3.69	3.00×10^{-2}	1.8×10^{-7}
170	534.1	3.69	3.00×10^{-2}	1.8×10^{-8}
340	1068	3.69	3.00×10^{-2}	2.3×10^{-9}
700	2199	3.69	3.00×10^{-2}	2.6×10^{-10}

TABLE II. Overview of the transmission at selected wavelength of the investigated materials and a thickness of 1.5 mm.

Material	$\lambda = 2\,\mu$m	$\lambda = 40\,\mu$m	$\lambda = 200\,\mu$m	$\lambda = 500\,\mu$m	$\lambda = 700\,\mu$m
SP0.45-80	$3.8(3.3) \times 10^{-4}$	$< 8.1 \times 10^{-4}$	$1.1(7) \times 10^{-4}$	$5.7(7) \times 10^{-4}$	$6.8(7) \times 10^{-3}$
SP0.45-700	$<4.4 \times 10^{-5}$	$<8.1 \times 10^{-4}$	$<5.3 \times 10^{-5}$	$8.7(6) \times 10^{-3}$	$3.24(23) \times 10^{-2}$
SP180 μm	$1.4(5) \times 10^{-3}$	$<8.1 \times 10^{-4}$	$<5.3 \times 10^{-5}$	$<5.7 \times 10^{-5}$	$1.18(13) \times 10^{-2}$
SP340 μm	$3.1(4) \times 10^{-3}$	$<8.1 \times 10^{-4}$	$<5.3 \times 10^{-5}$	$2.7(1.8) \times 10^{-4}$	$5.2(8) \times 10^{-4}$
SP700 μm	$7.5(5) \times 10^{-3}$	$<8.1 \times 10^{-4}$	$1.58(52) \times 10^{-4}$	$2.47(18) \times 10^{-3}$	$5.13(11) \times 10^{-3}$
PTFE	$4.63(5) \times 10^{-2}$	$2.09(29) \times 10^{-2}$	$7.5(8) \times 10^{-1}$	$8.90(24) \times 10^{-1}$	$8.29(22) \times 10^{-1}$
HDPE (transparent)	$3.96(5) \times 10^{-1}$	$8.23(8) \times 10^{-1}$	$8.84(18) \times 10^{-1}$	$8.87(21) \times 10^{-1}$	$8.98(25) \times 10^{-1}$
HDPE (black)	$<4.4 \times 10^{-5}$	$<8.1 \times 10^{-4}$	$1.67(2) \times 10^{-1}$	$4.92(11) \times 10^{-1}$	$6.06(17) \times 10^{-1}$
UHU plus Endfest 300	$2.89(11) \times 10^{-2}$	$8.2(7.6) \times 10^{-4}$	$5.15(14) \times 10^{-3}$	$1.72(7) \times 10^{-1}$	$3.32(13) \times 10^{-1}$
Stycast 2850FT	$<4.4 \times 10^{-5}$	$<8.1 \times 10^{-4}$	$1.51(10) \times 10^{-3}$	$9.9(4) \times 10^{-2}$	$1.93(8) \times 10^{-1}$
Eccosorb CR124	$<4.4 \times 10^{-5}$	$<8.1 \times 10^{-4}$	$<5.3 \times 10^{-5}$	$<5.7 \times 10^{-5}$	$8.4(1.6) \times 10^{-4}$
Copper powder	$<4.4 \times 10^{-5}$	$<8.1 \times 10^{-4}$	$<5.3 \times 10^{-5}$	$<5.7 \times 10^{-5}$	$<1.0 \times 10^{-4}$
Stainless steel powder	$<4.4 \times 10^{-5}$	$<8.1 \times 10^{-4}$	$<5.3 \times 10^{-5}$	$9.9(1.6) \times 10^{-4}$	$3.2(4) \times 10^{-2}$
Detector limit	4.4×10^{-5}	8.1×10^{-4}	5.3×10^{-5}	5.7×10^{-5}	1.0×10^{-4}

We now make the following approximations,[21,22] which are illustrated in Fig. 1(b): If radiation is scattered by several spheres with the same a, the total Q_{ext} should be additive. Similarly, we assume that the total Q_{ext} for a medium with a distribution of a will increase the extinction bandwidth.[22] This is shown by the solid black line in Fig. 1(d), which expresses the expected extinction coefficient $\mu_{ext,tot}$ in units of $1/\mu$m, given by

$$\mu_{ext,tot} = N_{tot} C_{ext,tot}, \tag{1}$$

where N_{tot} is the total number density per volume given for a mixture of equal masses by $N_{tot} = \sum_i 1/(\xi V_i(1 + \rho_{sapphire}/\rho_{epoxy}))$, and $C_{ext,tot} = \sum_i \gamma_i Q_{ext,i} \pi (a/2)^2$ the total extinction cross section; ξ is the number of different spheres in the mixture; the density ratio $\rho_{sapphire}/\rho_{epoxy} \approx 3.6$. The calculation of C_{ext} also includes a weighting factor $\gamma_i = V_i / \sum_j V_j$, which takes into account the relative number of individual spheres per volume.

We use commercially available[26] sapphire powders (SPs), Table I lists the median particle diameters assuming a spherical shape, the corresponding wavelength λ_x, where $x = 1$, the real and imaginary parts of the refractive index[25] $n(\lambda)$, $\kappa(\lambda)$, and weighting factor γ. The primary mixtures investigated are SP0.45-80 ($\xi = 5$) and SP0.45-700 ($\xi = 8$). All investigated sapphire–epoxy composites are nontransparent in the optical range.

To assess the IR blocking regime, we measured the infrared absorption of electromagnetic radiation with the wavelength between 1 and 1000 μm for various materials (Table II) using a commercial IR spectrometer. The supplementary material provide details on the measurement setup. Unless otherwise noted, the samples have a thickness of 1.5 mm (see the supplementary material). The absorption is compared in Fig. 2, please note the different scales. At wavelengths below 200 μm, the SP0.45-80 and SP0.45-700 compounds are nearly fully absorbing, dominated by the 0.45–80 μm spheres. In the FIR range (200–1000 μm), absorption decreases, consistent with the Rayleigh scattering limit for wavelengths larger than the largest grain size in the mixtures. The higher absorption of SP0.45-80 compared to SP0.45-700 will be discussed below.

Sample compounds consisting of single-diameter spheres [Fig. 2(b)] also show high absorption. The 170 μm sample approaches the Rayleigh scattering limit at $\lambda \approx 500\,\mu$m, resulting in reduced absorption. This limit is expected for spheres with diameters of 340

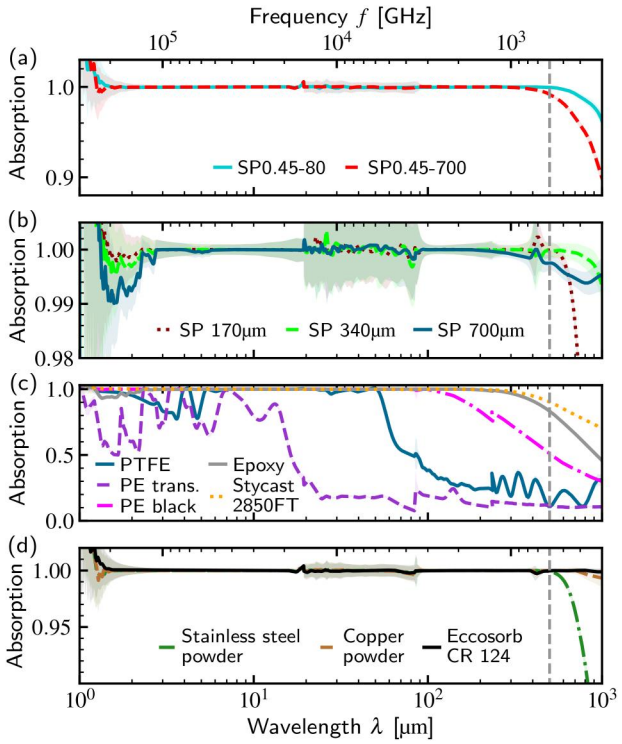

FIG. 2. Absorption spectra of various materials at a thickness of 1.5 mm. Please note the different scales. The gray dashed line illustrates the region shown in Fig. 4. (a) Sapphire powder mixtures SP0.45-80 and SP0.45-700, and epoxy resin. (b) Single-diameter sapphire powder samples. (c) PTFE, HDPE (transparent and black), Epoxy UHU+ Endfest 300, and Stycast 2850FT. (d) Eccosorb CR124 and epoxy resin mixed with metal powders (copper and stainless steel).

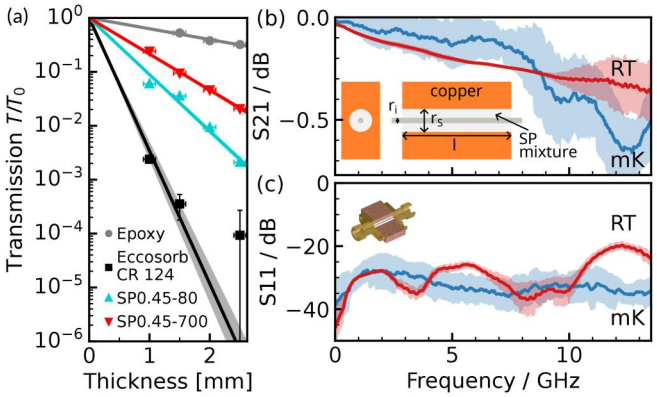

FIG. 3. (a) Transmission as a function of thickness at 864 μm for the SP mixtures, epoxy resin, and Eccosorb CR124. The solid line is a fit based on the Beer–Lambert law. (b) and (c) VNA transmission and reflection measurements of an filter implementation based on the SP0.45-700 compound. The insets show the schematics ($r_i = 0.4$ mm, $r_s = 2.2$ mm, and $l = 8$ mm). Red lines represent the measurements at room temperature (RT), blue at 15 mK.

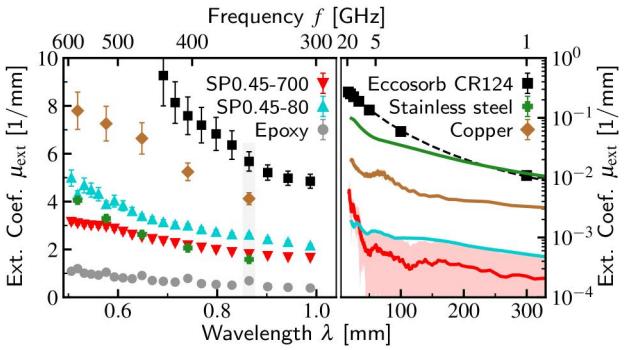

FIG. 4. The extinction coefficients of SP, epoxy resin, and Eccosorb CR124 are shown as a function of wavelength. The left graph shows the infrared range [gray region indicates the exemplary fit at 864 μm in Fig. 3(a)]. The right graph shows microwave data of the SP compound based filter shown in Figs. 3(b) and 3(c) as well as for copper and stainless steel. The Eccosorb CR124 data are taken from Ref. 28. Note the different y-scales on the left and right graphs.

and 700 μm, at wavelengths of approximately 1070 and 2200 μm, respectively [see Fig. 1(d)].

The absorption of PTFE, HDPE, Stycast 2850FT, Eccosorb CR124, and UHU plus Endfest 300 samples mixed with copper as well as stainless steel powders (mass ratio 1:2) is shown in Figs. 2(c) and 2(d).

HDPE (transparent) and PTFE show very low absorption, predominantly in the FIR region, demonstrating that they are indeed transparent to most thermal infrared radiation. For HDPE (black) (likely with a carbon filler), radiation is nearly completely blocked in the low MIR range (between 1 and 200 μm) and increased toward the FIR range. Stycast 2850FT and epoxy resin show a high MIR absorption, with increasing transmission at higher wavelengths. The metal powder samples and Eccosorb CR124 exhibit the highest absorption of the tested materials in the full IR range, extending even to the microwave regime, see the discussion below. They do not reach the typical asymptotic Rayleigh limit.

By measuring the samples at different thicknesses (1, 2, and 2.5 mm), we can fit the Beer–Lambert law to obtain the wavelength-dependent extinction coefficient μ_{ext} for each material (see the supplementary material). In Fig. 3(a), this is shown for an exemplary wavelength of 864 μm for the SP mixtures, epoxy resin, and Eccosorb CR124.

We expect no significant change at cryogenic temperatures for the SP material in the infrared range, as the strong interaction of Mie scattering is only weakly temperature dependent and arises from changes in the refractive index, thermal expansion, and the material's polarizability (order 10%), visible predominately around the resonant wavelength near 25 μm.[25,27] The situation in the microwave regime, however, is temperature dependent due to the material's thermal contraction and the changed dielectric constant.

To test this, filter prototypes were designed and built specifically for the SP0.45-700 compound, as illustrated in Fig. 3. We optimized the dimensions to match the 50 Ω impedance of the microwave network, particularly for the Kelvin and millikelvin temperature ranges (see the supplementary material). This can be seen in Figs. 3(b) and 3(c), where the reflection of cold samples shows a much flatter response around −30 dB in the range of 0–14 GHz and lower attenuation, e.g., at 5 GHz of 0.1 dB (mK) vs 0.2 dB (RT), with only small variations between different samples. The extracted filter impedances are 52.8 Ω (RT) and 51.9 Ω (mK) at 10 GHz, which deviate slightly from the target value but are sufficient for quantum applications. From this, we extract a small dielectric constant change from $\epsilon_r = 3.75$ (RT) to $\epsilon_r = 3.88$ (mK).

Figure 4 revisits the initial requirements of the low-pass filter. The critical FIR region, which is below $\lambda = 1.0$ mm (the limit of the IR setup), is compared with the transmission at microwave frequencies. Materials such as copper powder, stainless steel powder, or Eccosorb CR124 exhibit the anticipated high absorption, approximately two times higher than the SP compounds. Based on the measurement data, we estimate a lower bound of absorption for the SP compounds of 1.2×10^{-6} (118 dB) for $l = 8$ mm and $\lambda = 1,0$ mm. We note that the extinction data for the SP0.45-700 compound is lower than that of the SP0.45-80 compound due to a finite-size effect in the IR absorption measurement: The 170, 340, and 700 μm sapphire spheres occupy a large volume within the 1–2.5 mm thick samples, leading to a low number of scattering events [see Fig. 3(a)]. In a real filter with $l \gg 2.5$ mm, the number of Mie scattering events is substantially higher, making it more efficient.

In the passband at 9 GHz ($\lambda = 33.3$ mm), as shown in Fig. 4 (right), we find that the extinction coefficient is approximately $\mu_{ext} \approx 1.9 \times 10^{-3}$/mm for the SP0.45-700 compound and approximately 1.9×10^{-1} /mm for Eccosorb CR124.

In summary, we propose a non-magnetic material compound consisting of epoxy resin and sapphire spheres of adapted sizes to achieve high infrared attenuation (stop band) and minimal attenuation in the microwave range (passband). We simulated the composition using Mie scattering theory, which is useful for estimating the extinction length in the case of strong photon–sphere interaction. The simulation predictions were tested using infrared absorption measurements on the material system, and compared to several conventional materials used in low-temperature quantum applications. The experimental results confirm the desired low-pass behavior, demonstrating absorption exceeding $\mu_{ext} \approx 2$/mm up to far-infrared

wavelengths and $\mu_{ext} \approx 4 \times 10^{-4}$/mm in the GHz regime. A low-pass filter prototype made from the SP0.45-700 compound was tested at millikelvin temperatures. Compared with measured metallic powders of copper and stainless steel, SP0.45-700 shows a similar stop band attenuation and about 25× lower passband attenuation up to 10 GHz.

See the supplementary material for additional details on Mie scattering simulations (A), the filter material and sample preparation (B), IR measurement and data processing (C), microwave measurement details (D), and additional IR measurement data (E). It includes Refs. 22 and 24–26.

We acknowledge technical lab support by Sebastian Koch and Rebecca Zwickel. This research was supported by the German Federal Ministry of Education and Research under the Research Program Quantum Systems through the projects GeQCoS (No. FZK13N15691), qBriqs (No. FZK13N15950), and Qrious (No. FZK13N17125) as well as by funding from the European Research Council (ERC Advanced Grant *Milli-Q*, GAN101054327).

AUTHOR DECLARATIONS

Conflict of Interest

The authors have no conflicts to disclose.

Author Contributions

Markus Griedel: Conceptualization (equal); Formal analysis (equal); Investigation (equal); Methodology (equal); Validation (equal); Visualization (equal); Writing – original draft (equal); Writing – review & editing (equal). **Max Kristen:** Investigation (supporting); Writing – review & editing (equal). **Biliana Gasharova:** Investigation (supporting); Writing – review & editing (equal). **Yves-Laurent Mathis:** Investigation (supporting); Writing – review & editing (equal). **Alexey V. Ustinov:** Funding acquisition (equal); Supervision (equal); Writing – review & editing (equal). **Hannes Rotzinger:** Conceptualization (equal); Formal analysis (equal); Funding acquisition (equal); Investigation (equal); Methodology (equal); Project administration (equal); Resources (equal); Supervision (equal); Validation (equal); Writing – original draft (equal); Writing – review & editing (equal).

DATA AVAILABILITY

The data that support the findings of this study are available from the corresponding author upon reasonable request.

REFERENCES

[1]F. C. Wellstood, C. Urbina, and J. Clarke, Appl. Phys. Lett. **50**, 772 (1987).
[2]D. Drung, J. Beyer, J.-H. Storm, M. Peters, and T. Schurig, IEEE Trans. Appl. Supercond. **21**, 340 (2011).
[3]R. Barends, J. Wenner, M. Lenander, Y. Chen, R. C. Bialczak, J. Kelly, E. Lucero, P. O'Malley, M. Mariantoni, D. Sank, H. Wang, T. C. White, Y. Yin, J. Zhao, A. N. Cleland, J. M. Martinis, and J. J. A. Baselmans, Appl. Phys. Lett. **99**, 113507 (2011).
[4]P. J. de Visser, J. J. A. Baselmans, S. J. C. Yates, P. Diener, A. Endo, and T. M. Klapwijk, Appl. Phys. Lett. **100**, 162601 (2012).
[5]C. Wang, Y. Y. Gao, I. M. Pop, U. Vool, C. Axline, T. Brecht, R. W. Heeres, L. Frunzio, M. H. Devoret, G. Catelani, L. I. Glazman, and R. J. Schoelkopf, Nat. Commun. **5**, 5836 (2014).
[6]S. Gustavsson, F. Yan, G. Catelani, J. Bylander, A. Kamal, J. Birenbaum, D. Hover, D. Rosenberg, G. Samach, A. P. Sears, S. J. Weber, J. L. Yoder, J. Clarke, A. J. Kerman, F. Yoshihara, Y. Nakamura, T. P. Orlando, and W. D. Oliver, Science **354**, 1573 (2016).
[7]E. T. Mannila, P. Samuelsson, S. Simbierowicz, J. T. Peltonen, V. Vesterinen, L. Grönberg, J. Hassel, V. F. Maisi, and J. P. Pekola, Nat. Phys. **18**, 145 (2022).
[8]C. H. Liu, D. C. Harrison, S. Patel, C. D. Wilen, O. Rafferty, A. Shearrow, A. Ballard, V. Iaia, J. Ku, B. L. T. Plourde, and R. McDermott, Phys. Rev. Lett. **132**, 017001 (2024).
[9]R. Benevides, M. Drimmer, G. Bisson, F. Adinolfi, U. v Lüpke, H. M. Doeleman, G. Catelani, and Y. Chu, Phys. Rev. Lett. **133**, 060602 (2024).
[10]A. Lukashenko and A. V. Ustinov, Rev. Sci. Instrum. **79**, 014701 (2008).
[11]J. M. Kreikebaum, A. Dove, W. Livingston, E. Kim, and I. Siddiqi, Supercond. Sci. Technol. **29**, 104002 (2016).
[12]S. Danilin, J. Barbosa, M. Farage, Z. Zhao, X. Shang, J. Burnett, N. Ridler, C. Li, and M. Weides, EPJ Quantum Technol. **9**, 1 (2022).
[13]A. Paquette, J. Griesmar, G. Lavoie, R. Albert, F. Blanchet, A. Grimm, U. Martel, and M. Hofheinz, Appl. Phys. Lett. **121**, 124001 (2022).
[14]A. I. Ivanov, V. I. Polozov, V. V. Echeistov, A. A. Samoylov, E. I. Malevannaya, A. R. Matanin, N. S. Smirnov, and I. A. Rodionov, Appl. Phys. Lett. **123**, 204001 (2023).
[15]Laird, see https://www.laird.com/sites/default/files/2021-01/RFP-DS-CRS%2006242020.pdf for "Eccosorb®CRS Datasheet" (last accessed December 19, 2025).
[16]T. Essinger-Hileman, C. L. Bennett, L. Corbett, H. Guo, K. Helson, T. Marriage, M. A. B. Meador, K. Rostem, and E. J. Wollack, Appl. Opt. **59**, 5439 (2020).
[17]K. R. Helson, S. Arseneau, A. Barlis, C. L. Bennett, T. M. Essinger-Hileman, H. Guo, T. Marriage, M. A. Quijada, A. E. Tokarz, S. L. Vivod, and E. J. Wollack, "Novel infrared-blocking aerogel scattering filters and their applications in astrophysical and planetary science," arXiv:2208.03755 (2022).
[18]J. Krupka, K. Derzakowski, A. Abramowicz, M. Tobar, and R. Geyer, IEEE Trans. Microwave Theory Tech. **47**, 752 (1999).
[19]M. Kudra, J. Biznárová, A. Fadavi Roudsari, J. J. Burnett, D. Niepce, S. Gasparinetti, B. Wickman, and P. Delsing, Appl. Phys. Lett. **117**, 070601 (2020).
[20]A. Beer, Ann. Phys. Chem. **162**, 78 (1852).
[21]M. Kerker, *The Scattering of Light and Other Electromagnetic Radiation*, Physical Chemistry: A Series of Monographs Vol. 16, edited by M. Kerker (Academic Press, 1969), pp. 27–96.
[22]C. F. Bohren and D. R. Huffman, *Absorption and Scattering of Light by Small Particles*, 1st ed. (Wiley, 1998).
[23]S. Prahl (2024). "Miepython: Pure python calculation of Mie scattering," Zenodo. https://doi.org/10.5281/ZENODO.14257432
[24]UHU, see https://dosieren.de/media/2d/fc/1b/1631520815/uhu_end_50n_tds_de.pdf for "Plus Endfest 300 Datenblatt" (last accessed December 19, 2025).
[25]M. R. Querry, "Optical constants," Report No. CRDC-CR-85034 [University of Missouri; U.S. Army Chemical Research and Development Center (CRDC), Kansas City, Missouri, 1985].
[26]Final Advanced Materials, see https://www.final-materials.com/gb/index.php?controller=attachment&id_attachment=115 for "2MS.001 FINAL Advanced Materials – Alumina Powder" (last accessed December 19, 2025).
[27]M. Halpern, H. P. Gush, E. Wishnow, and V. D. Cosmo, Appl. Opt. **25**, 565 (1986).
[28]Laird, see https://www.laird.com/sites/default/files/2021-07/RFP-DS-MF%20061721.pdf for "Eccosorb®MF datasheet" (last accessed December 19, 2025).